Solid State Sciences 22 (2013) 27–32

Contents lists available at SciVerse ScienceDirect

Solid State Sciences

journal homepage: www.elsevier.com/locate/ssscie

LPG sensing application of graphene/Bi_2O_3 quantum dots composites

K.R. Nemade, S.A. Waghuley*

Department of Physics, Sant Gadge Baba Amravati University, Amravati 444 602, India

ARTICLE INFO

Article history:
Received 16 April 2013
Received in revised form
7 May 2013
Accepted 9 May 2013
Available online 24 May 2013

Keywords:
Graphene
Bi_2O_3
LPG

ABSTRACT

Liquid petroleum gas (LPG) sensing characteristics of graphene/Bi_2O_3 quantum dots (QDs) composites have been studied. The prepared materials were characterized through X-ray diffraction, atomic force microscopy, Raman, high resolution-transmission electron microscopy along with selected area electron diffraction, ultraviolet–visible spectroscopy, fluorescence spectroscopy and thermo gravimetric-differential thermal analysis. The X-ray diffraction pattern of Bi_2O_3 showed broad peaks and intense absorption at 362 nm in UV–VIS spectrum confirms that chemically synthesized Bi_2O_3 particles are quantum dots. The composites show significant better performance towards the LPG. The defects chemistry was employed to analyse the increasing gas sensing properties with an increasing wt.% of graphene. Also, excellent correlation observed between the defects concentration (I_{UV}/I_{DL}) and sensing response as a function of wt.% of graphene.

1. Introduction

LPG is a very competent energy source that burns in a clean way, but due to extremely flammable nature this gas is hazards to humans [1]. LPG is invisible and has no natural smell, so a unique smell is added to make possible any leaks to be detected. Due to its highly explosive nature, even for low concentration (ppm) creates serious problem [2]. Hence, it is important to detect it at its lower concentration very efficiently. Metal oxide based LPG sensors enables to detect lower concentration of LPG presence, but suffer from lack of selectivity and high operation temperature [3]. The detection of LPG at higher temperature increases power consumption and risk [4]. For this, many efforts are made by researchers to investigate novel LPG sensing materials. Gurav et al. reported the LPG sensing using Pd-sensitized vertically aligned ZnO nanorods [5] with operating temperature 573 K. Hence, the present work is a bold attempt to resolve high temperature operation disadvantage using novel material graphene/Bi_2O_3 composite.

As a potential candidate in material science, graphene has excellent gas sensing properties due to its high surface to volume ratio [6]. Schedin et al. reported graphene based FET (field-effect transistors) to detect the absorption of a single gas molecule [7]. The Bi_2O_3 is much more known transition metal oxide semiconductor. It has been extensively investigated for various applications as photocatalyst [8], ion conducting solid electrolyte [9], optical and electrical material in solid oxide fuel cells [10] and oxygen sensors [11], and selective sensing material for NO detection [12]. In the last decade, Bi_2O_3 has been reported with various morphologies, such as nanorods [13], nanotubes [14], nanowires [15] and nanofibers [16]. Due to such morphology, Bi_2O_3 has found numerous modern applications in electronics and electro-optics [17–20], catalysis [21] and gas sensors [11].

In the present work, for the first time, we explored the LPG sensing properties of graphene/Bi_2O_3 composite. Much effort has been put to reduce operating temperature in order to reduce operation cost and risk. The structural, morphological, optical and thermal properties of graphene/Bi_2O_3 composite were investigated using X-ray diffraction (XRD), atomic force microscopy (AFM), Raman, high resolution-transmission electron microscopy (HR-TEM)-selected area diffraction pattern (TEM-SAED), ultraviolet–visible (UV–VIS) spectroscopy, fluorescence spectroscopy and thermo gravimetric-differential thermal analysis (TG-DTA).

2. Experimental

The Bi_2O_3 QDs were obtained through chemical route. In a typical experiment, precursors bismuth nitrate (1 M) and hexamethylenetetramine (HMT) (1 M) were dissolved in 30 ml double distilled water separately. The solutions were mixed thoroughly by addition of HMT drop-by-drop under magnetic stirring for 2 h at room temperature. Subsequently, the product was kept for a centrifuge operating at 3000 rpm for 30 min. This centrifuged precipitate was collected through cellulose nitrate filter paper. The

* Corresponding author. Tel.: +91 9423124882.
E-mail address: sandeepwaghuley@sgbau.ac.in (S.A. Waghuley).

1293-2558/$ – see front matter © 2013 Elsevier Masson SAS. All rights reserved.
http://dx.doi.org/10.1016/j.solidstatesciences.2013.05.008

filtrate was dried at room temperature for over night in vacuum chamber and then sintered at 373 K for 3 h.

The electrochemical exfoliation method was used to synthesize graphene; during the process silver was used as a cathode and graphite flake as anode. The electrodes were inserted into the ionic solution with separation of 5 cm. The ionic solution was prepared by taking 4.8 g of sulphuric acid diluted in 100 ml of double distilled water [22]. Exfoliation process was carried out by DC bias arrangement (10 V) at room temperature. The prepared graphene was collected through cellulose nitrate filter paper and washed with double distilled water several times. The obtained sample was dried at 373 K for 2 h.

The graphene/Bi_2O_3 QDs composites were prepared by mixing graphene in constant 1 g Bi_2O_3 QDs, where acetone used as organic media. The solution was thoroughly mixed by magnetic stirrer for 30 min at room temperature. The resultant solution was kept for over night for evaporation of acetone. In this manner, prepared composite was sintered at 373 K for 1 h. During this stage, complete evaporation of acetone takes place. Same method was employed to prepare composite with varying wt.% of graphene from 20 to 80 wt.%.

The X-ray diffraction (XRD) patterns of samples were recorded on an XRD Philips PW 1830 using CuK_α radiation ($\lambda = 1.54$ Å) in the range 1060°. The morphology of the samples was studied using imaging techniques, high resolution-transmission electron microscopy (HR-TEM)- selected area electron diffraction (SAED) (Philips Tecnai F-30107). The surface topography and thickness distribution of graphene was observed by AFM on Bruker Webinar Series. Raman spectra was acquired on a BRUKER RFS 27: Raman Spectrometer using Nd: YAG laser source of excitation 514 nm. The optical transmission was measured by a UV–VIS spectrophotometer (Perkin Elmer) for the conformation of quantum confinement. The fluorescence analysis was done on FL Spectrophotometer (Model: HITACHI, F-7000) to know the defects density. The thermal stability of material analysed through thermo gravimetric-differential thermal analysis (TG-DTA) on Shimadzu DTG-60h thermal analyser under nitrogen atmosphere.

The chemiresistor films for LPG sensing were prepared by screen-printing on glass substrate of size 25 mm × 25 mm and then dried at room temperature for 24 h [23]. The heating treatment was given to the film at 373 K for 3 h. For surface resistance measurement, the electrodes of silver were deposited on adjacent sides of the film and then it was kept to heating at 353 K for 15 min for drying the silver paint. The sensing response was determined from resistance change of chemiresistor. The electrical resistance was measured by using a voltage drop method adopted by Waghuley et al. [23]. The gas sensing response of chemiresistor is defined as

$$S = \frac{\Delta R}{R_a} = \frac{|R_g - R_a|}{R_a} \quad (1)$$

where R_a is the resistance of chemiresistor in air and R_g is the resistance chemiresistor in gas. The response time was determined by injecting known amount of gas in the chamber. The time taken by chemiresistor to achieve 90% of its highest value was considered as response time. While, the recovery time of the chemiresistor was defined as the time taken for its resistance to be reduced by 90% from its highest value. The experiment was carried out 5 times for reproducibility of chemiresistors.

3. Results and discussion

3.1. Materials characterization

Fig. 1(a)–(f) depicts the XRD patterns of graphene and Bi_2O_3 QDs along with (20–80 wt.%) graphene/Bi_2O_3 QDs composites. The XRD

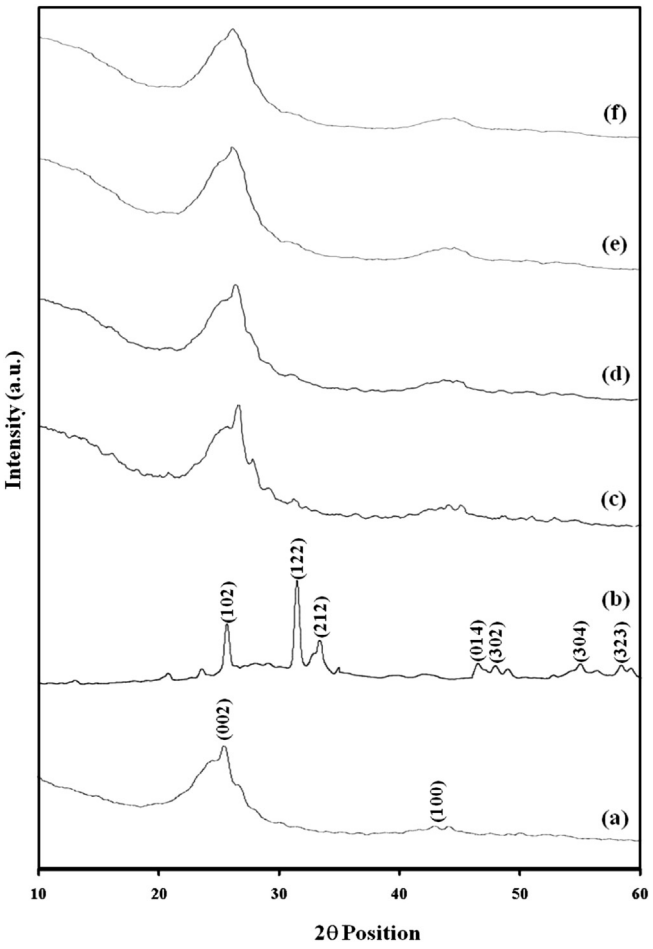

Fig. 1. XRD patterns of (a) graphene, (b) Bi_2O_3 QDs and (c) 20 wt.%, (d) 40 wt.%, (e) 60 wt.% and (f) 80 wt.% graphene/Bi_2O_3 QDs composites.

pattern shown in Fig. 1 (a), indicates the formation of graphene. There are two prominent peaks (002) and (100) which are characteristic peaks of graphene [24]. Fig. 1(b) shows the structural purity of Bi_2O_3 QDs. There are seven prominent peaks observed in the XRD pattern, (102), (122), (212), (014), (302), (304), and (323) which are characteristic peaks of Bi_2O_3 QDs. All the peaks exactly match with JCPDS Data Card No. 41-1449. The XRD pattern of composites shows in Fig. 1 (c)–(f) displays broad hump peak, which implies that the composites are nanocrystalline or loose the crystallites [25]. This loose crystallites may be due addition of graphene in Bi_2O_3 induce disorder/defects in the structure [26,27]. The crystallite size decreases with an increase in the wt.% of graphene. Debye–Scherrer formula was used to calculate the crystallite size. The average crystallite size of Bi_2O_3 QDs was found to be 4.63 nm and for composites, it was found to be ranges between the 5.23 and 5.68 nm. The smallest crystallite size was found to be 5.23 nm for 80 wt.% graphene/Bi_2O_3 QDs composite. The crystallite size of composites does not show significant difference.

Fig. 2(a) shows AFM image and thickness profile of graphene. The thickness distribution of graphene was 1.77 nm, indicated the few layered structure of graphene possesses 5–6 layers. The Raman spectrum of graphene is shown in Fig. 2(b). The prominent Raman features of FLG are D-band ($\sim$1300 cm^{-1}), G-band ($\sim$1580 cm^{-1}) and 2D-band ($\sim$2700 cm^{-1}). The D-band is known as the defect concentration band. The intensity of the D-band is directly proportional to the concentration of defects. The G-band assigned to in-plane vibration of sp^2 carbon atoms [28]. The 2D-band originates from a two-phonon double resonance process [29].

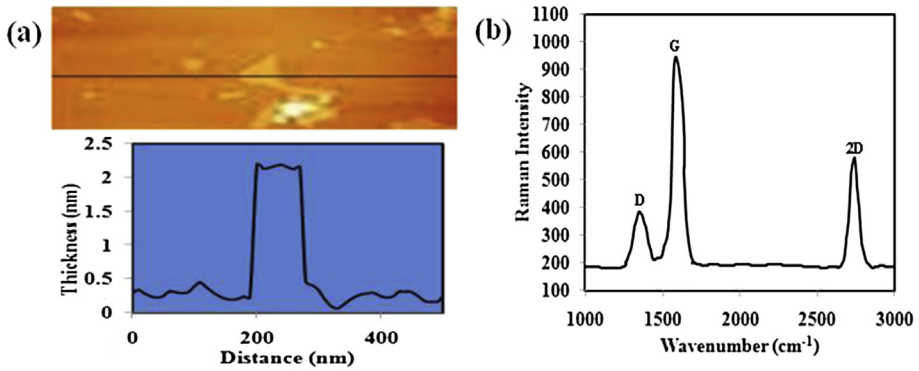

Fig. 2. (a) AFM image with thickness distribution of graphene and (b) Raman spectrum of graphene.

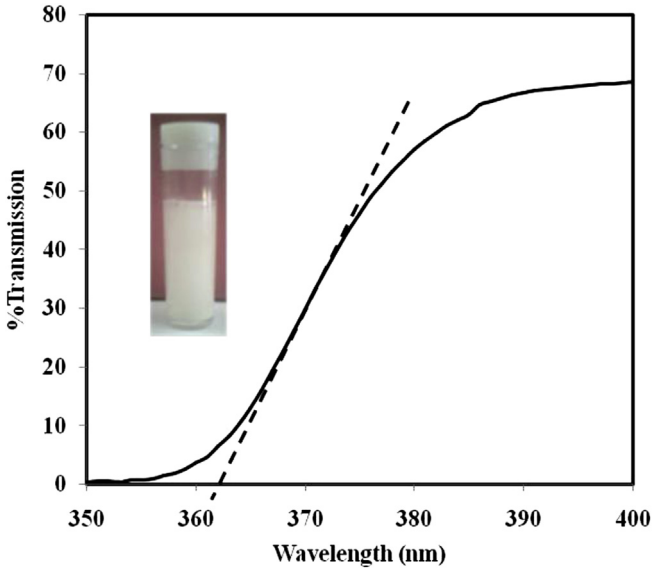

Fig. 3. UV–VIS spectra of the Bi_2O_3 QDs dispersed in distilled water. Inset shows the optical photograph.

Fig. 3 shows UV–VIS spectrum of Bi_2O_3 QDs. The plots show intense absorption at 362 nm. This absorption in UV region confirms the presence of quantum confinement.

The morphology of as-prepared graphene was examined through TEM; representative image is shown in Fig. 4(a). The TEM image of graphene shows a wrinkled sheet like structure at the edges. Inset of Fig. 4(a) shows the SAED image of graphene. The planes appeared in SAED image are agreed with the results obtained from XRD analysis. The SAED image is clearly visible, and the bright diffraction spots reflect the hexagonal symmetry [30]. Fig. 4(b) presents the TEM image of Bi_2O_3 QDs. TEM image shows the small amount of aggregation of Bi_2O_3 QDs. The average crystallite size of Bi_2O_3 QDs estimated from XRD analysis agrees with

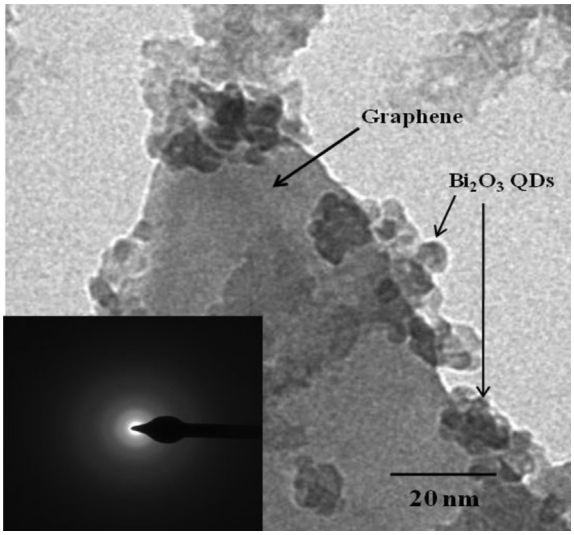

Fig. 5. TEM and SAED image of 80 wt.% graphene/Bi_2O_3 QDs composite.

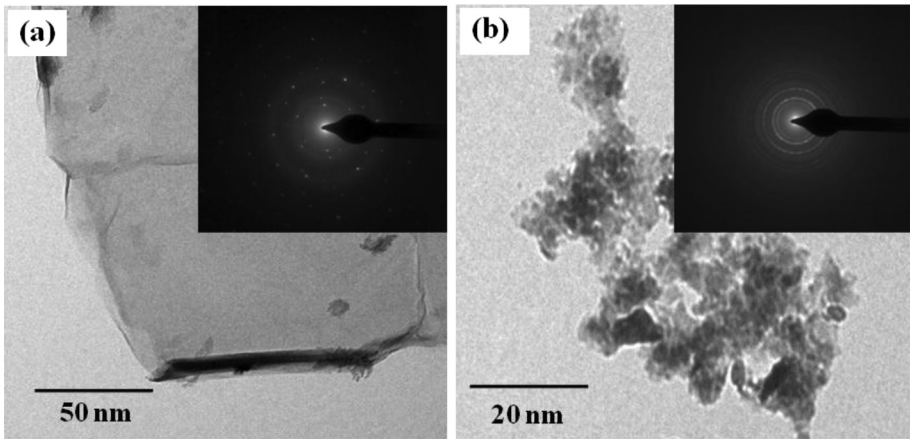

Fig. 4. (a) TEM image of graphene and inset shows the SAED image. (b) TEM image of Bi_2O_3 QDs shows the aggregation of particles and inset shows the SAED image.

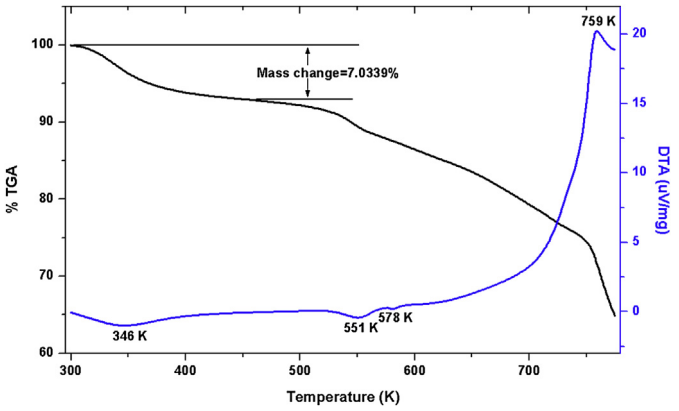

Fig. 6. TG–DTA curves of 80 wt.% graphene/Bi_2O_3 QDs composites.

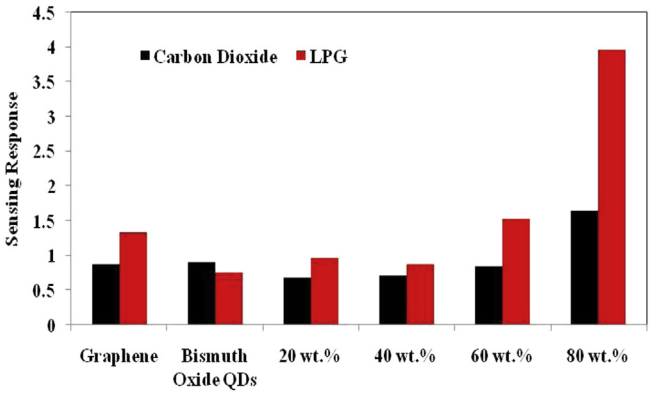

Fig. 8. Response of chemiresistors towards CO_2 (30 ppm) and LPG (30 ppm) at 398 K.

TEM investigation. The inset image shows the SAED image, which is consistent with the diffraction planes obtained from XRD analysis.

The HR-TEM image of the 80 wt.% graphene/Bi_2O_3 QDs composite provided in Fig. 5. This image shows hybridised structure of graphene and Bi_2O_3 QDs. The inset of Fig. 5 shows the SAED image of composite; reflects composite possesses less crystalline or amorphous structure. This result is consistent with XRD analysis.

Fig. 6 demonstrates the TG-DTA of 80 wt.% graphene/Bi_2O_3 QDs composites, in order to study the changes occurred regarding the phase transition during heat treatment to the sample. The TG-DTA analysis was carried out from room temperature to 775 K in nitrogen atmosphere.

According to the % TGA curve, the sample shows sharp weight loss upto 373 K and DTA shows an endothermic pick at 346 K corresponding to the evaporation of absorbed water. The total mass loss from room temperature to 453 K was about 7.0339%. The DTA curve shows another peak at 551 K, corresponds to the evaporation of the constitution water in Bi_2O_3 QDs. The weak peak at 578 K assigned to the oxidation of amorphous carbon present on the surface of graphene [31]. The exothermic peak appears at 759 K, which may be associated with the phase transition from α-Bi_2O_3 → δ-Bi_2O_3 in composite [32]. The thermal study of sample shows the stability of composite material in the vicinity of operating temperature of 80 wt.% graphene/Bi_2O_3 QDs composites chemiresistor.

The sensing characteristics are significantly influence by defects concentration on the sensing surface [33,34]. Thus, the fluorescence spectroscopy is straightforward approach of measurements of defects density. Fig. 7 shows the fluorescence spectrum of (20–80 wt.%) graphene/Bi_2O_3 QDs composites. From plots, it is observed that the intensity value of ultraviolet (I_{UV}) enhanced with an increase in wt.% of graphene. This shows that the graphene surface becomes defects rich in the presence of Bi_2O_3 QDs. The intensities ratio of the ultraviolet (I_{UV}) to visible leep levels (I_{DL}) is measure of defect concentration [34].

3.2. LPG sensing characteristics

The capability of a chemiresistor to respond to a definite gas is known as selectivity. The selectivity response of chemiresistors was checked towards to 30 ppm CO_2 and LPG at 398 K. The results are shows in Fig. 8. The composites are more selective towards the LPG, than CO_2. It is clearly observable that 80 wt.% graphene/Bi_2O_3 composites chemiresistor is highly selective.

As the composite chemiresistors are more selective towards the LPG, the sensing response of chemiresistors was measured as a function of concentration of LPG at room temperature (303 K). The results are presented in Fig. 9. The chemiresistors shows an increase in response as a function of LPG concentration upto 100 ppm. Beyond 100 ppm, response of chemiresistors decline from linearness. This suggested the saturation effect of chemiresistors. From the plots, it is observed that 80 wt.% graphene/Bi_2O_3 composite highly responsive even at room temperature. This may be due the smaller crystallite size, which provides a larger surface

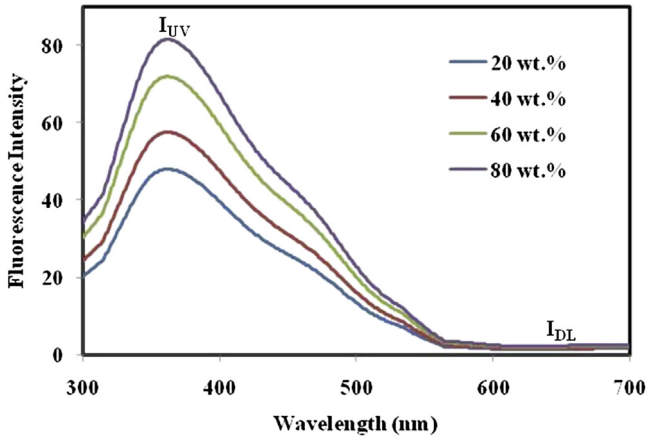

Fig. 7. Fluorescence spectrum of (20–80 wt.%) graphene/Bi_2O_3 QDs composites.

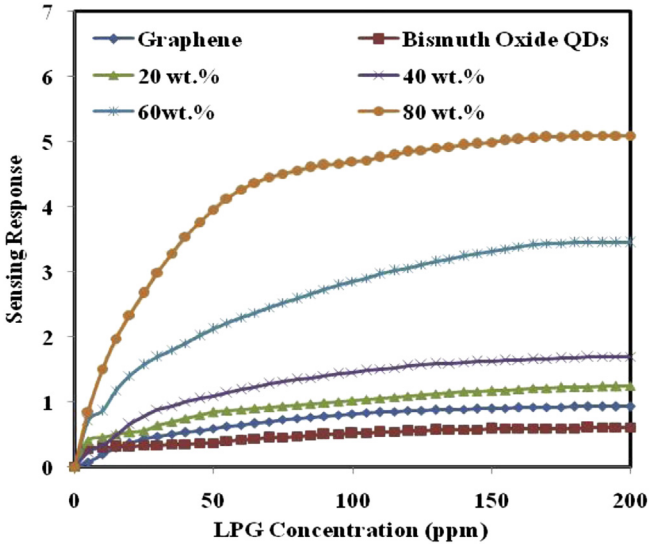

Fig. 9. Chemiresistor response as a function of concentration of LPG.

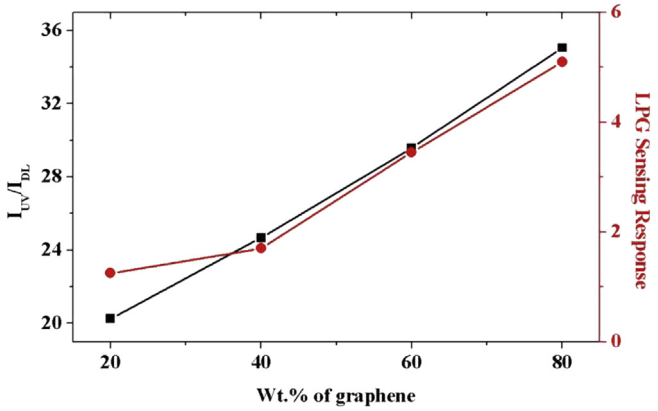

Fig. 10. The variation of defects density (I_{UV}/I_{DL}) ratio and LPG sensing response with the wt.% of graphene.

to volume ratio for gas–solid interaction [35]. An additional reason for increase in response with wt.% of graphene attributed to an increase in defects concentration. Fig. 10 shows the variation of defects density (I_{UV}/I_{DL}) ratio and LPG sensing response as a function of wt.% graphene. From the plots, it is analysed that LPG response increases linearly with defects concentration and wt.% graphene. This result is consistent well with the [34].

Gas sensing action basically depends on electron transfer reactions, which are redox reactions. The free energy that drives the reaction is the difference in reduction potentials between donor and acceptor [36]. As mentioned above, gas sensing related to defects, that is oxygen vacancies can act as adsorption sites for gas molecules. The reactions for adsorbed oxygen ions are as follows (Eqs. (2)–(4)) [37].

$$O_2(gas) \rightarrow O_2(ads) \quad (2)$$

$$O_2(ads) + e^- \rightarrow O_2^-(ads) \quad (3)$$

$$O_2^-(ads) + e^- \rightarrow 2O^-(ads) \quad (4)$$

It is well known that LPG is composition of CH_4, C_3H_8, C_4H_{10}, etc., and these molecules having tendency to donate electron to the surface. When the chemiresistor is exposed to LPG, it interacts with the adsorbed oxygen ions and formed H_2O and CO_2. The reaction between LPG and adsorbed oxygen ions are as follows (Eqs. (5) and (6)) [35].

$$C_nH_{2n+2} + 2O^-(ads) \rightarrow H_2O + C_nH_{2n}{:}\ O + e^- \quad (5)$$

$$C_nH_{2n}{:}\quad O + O^-(ads) \rightarrow CO_2 + H_2O + e^- \quad (6)$$

The response of chemiresistors towards the 50 ppm LPG as a function of operating temperature is shown in Fig. 11. All curves shows a highest sensing response values corresponding to temperature. From the plot, it is examined that all composites possess low operating temperature at 398 K. The 80 wt.% graphene/Bi_2O_3 composites exhibited the optimum value of sensing response. This is the most important accomplishment of present investigation, which reduced the operation cost. Besides that, sensing of LPG at elevated temperature is tricky due to its explosive nature. This problem resolved up to some extent by present study. The response value start to decreases from certain temperature, this may be due to desorption of oxygen ions from sensing surface [37].

The primary sensing mechanism is applicable to pure graphene and Bi_2O_3 QDs, which is based on charge transfer between adsorbed gas molecules and sensing surface, leading to change in its resistance. It is known that a certain amount of oxygen from air is adsorbed on the surface of the chemiresistors. The graphene and Bi_2O_3 QDs interact simply with the oxygen, by transferring the electrons from the conduction band to adsorbed oxygen atoms. Therefore, the adsorption of LPG molecules on the sensing surface is the dominant sensing mechanism [38–40]. Careful analysis of sensing mechanism in case of composites shows that Bi_2O_3 QDs act as active sensing sites by damaging the graphene surface, which may create vacancies or dangling bonds on graphene surface and subsequently, enhance defects density [28].

In order to check the stability of 80 wt.% graphene/Bi_2O_3 composites, its responses to 100 ppm LPG was measured for 30 days at an interval of 5 days at room temperature. The results are illustrated in Fig. 12. The chemiresistors have nearly constant response to LPG indicating the good stability. The transient response characteristic of 80 wt.% graphene/Bi_2O_3 composite chemiresistor to 100 ppm LPG were studied at room temperature and displayed in inset of Fig. 12. In this measurement, gas inserted in the chamber and resistance of chemiresistor was measured in air and in

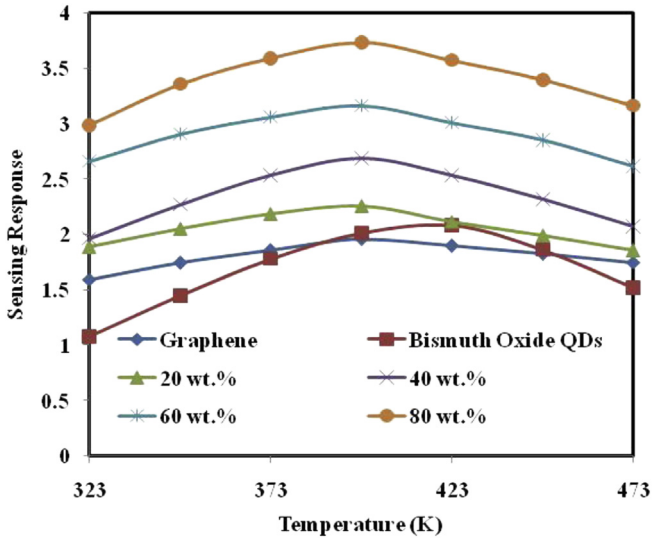

Fig. 11. Chemiresistor response as a function of operating temperature to 50 ppm LPG.

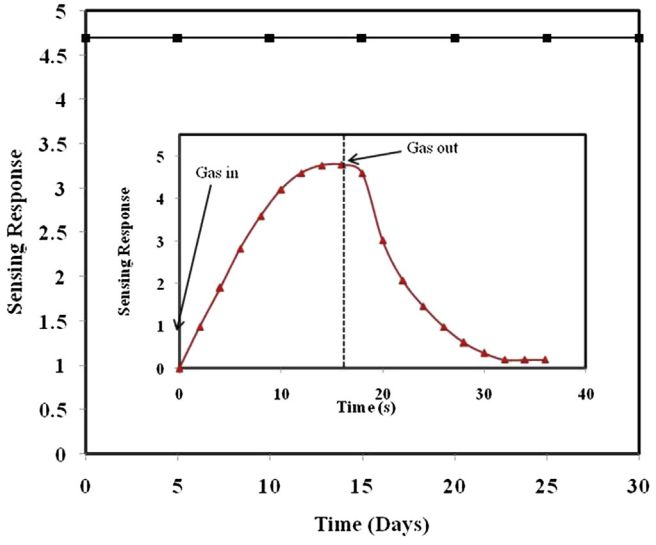

Fig. 12. Stability and transient response (inset) characteristics of 80 wt.% graphene/Bi_2O_3 QDs chemiresistor to 100 ppm LPG.

presence of gas. The 80 wt.% chemiresistor shows fast response time towards the LPG of the order 16 s. For measuring the recovery time, chemiresistor was exposed to air. The chemiresistor achieve fast recovery in 20 s. The results indicate that the chemiresistor can meet the practical application for detection of LPG.

On the basis of above discussion, it can be hypothesized that, as a general, increasing the graphene content in Bi_2O_3 enhances the sensing response to LPG. Obviously, a more detailed investigation is necessary to validate this hypothesis. Further work on enhancement of sensing response is currently under way.

4. Conclusions

The addition effect of graphene on LPG sensing properties of graphene/Bi_2O_3 QDs composites was successfully investigated. It was found that the addition of graphene into Bi_2O_3 QDs, makes graphene surface defective. This directly and simply confirmed using fluorescence spectroscopy. Simultaneously, provide strong support to improvement in LPG sensing properties based on defect density. The 80 wt.% graphene/Bi_2O_3 composite possesses high sensing response; low operating temperature, fast response and recovery time along with good stability are adequate to be a practical LPG sensor. Low operating temperature feature of 80 wt.% graphene/Bi_2O_3 composite chemiresistor reduced the operation cost as well as risk.

Acknowledgments

Authors are very much thankful to Head, Department of Physics Sant Gadge Baba Amravati University, Amravati, India for providing necessary facilities.

References

[1] D. Haridas, V. Gupta, K. Sreenivas, Bull. Mater. Sci. 31 (2008) 1–4.
[2] D.S. Dhawale, D.P. Dubal, A.M. More, T.P. Gujar, C.D. Lokhande, Sens. Actuators B 147 (2010) 488–494.
[3] J.L. Gunjakar, A.M. More, C.D. Lokhande, Sens. Actuators B 131 (2008) 356–361.
[4] R.R. Salunkhe, V.R. Shinde, C.D. Lokhande, Sens. Actuators B 133 (2008) 296–301.
[5] K.V. Gurav, P.R. Deshmukh, C.D. Lokhande, Sens. Actuators B 151 (2011) 365–369.
[6] H.E. Romero, P. Joshi, A.K. Gupta, H.R. Gutierrez, M.W. Cole, S.A. Tadigadapa, P.C. Eklund, Nanotechnology 20 (2009) 245,501.
[7] F. Schedin, A.K. Geim, S.V. Morozov, E.W. Hill, P. Blake, M.I. Katsnelson, K.S. Novoselov, Nat. Mater. 6 (2007) 652–655.
[8] M.J. Verkerk, K. Keizer, A.J. Burggraaf, J. Electrochem. Soc. 10 (1980) 70–78.
[9] P. Shuk, H.D. Wiemhofer, U. Guth, W. Gopel, M. Greenblatt, Solid State Ionics 89 (1996) 179–196.
[10] A.M. Azad, S. Larose, S.A. Akbar, J. Mat. Sci. 29 (1994) 4135–4151.
[11] A. Cabot, A. Marsal, J. Arbiol, J.R. Morante, Sens. Actuators B 99 (2004) 74–89.
[12] L.S. Zhang, W.Z. Wang, J. Yang, Z.G. Chen, W.Q. Zhang, L. Zhou, Appl. Catal. A 308 (2006) 105–110.
[13] H.W. Kim, J.W. Lee, S.H. Shim, Sens. Actuators B 126 (2007) 306–310.
[14] L. Li, Y.W. Yang, G.H. Li, L.D. Zhang, Small 2 (2006) 548–553.
[15] Y.F. Qiu, D.F. Liu, J.H. Yang, S.H. Yang, Adv. Mater. 18 (2006) 2604–2608.
[16] S. Wu, C. Wang, Y. Cui, T. Wang, B. Huang, X. Zhang, X. Qin, P. Brault, Mater. Lett. 64 (2010) 115–118.
[17] M. Miyayama, H. Yanagida, J. Mater. Sci. 21 (1986) 1233–1236.
[18] S.C. Abrahams, P.B. Jamienson, J.L. Bemstein, J. Chem. Phys. 47 (1976) 4034–4042.
[19] V. Tassev, G. Diankov, M. Gospodinov, Opt. Soc. Am. B 14 (1997) 1761–1764.
[20] P.S. Halasyamani, K.R. Poeppelmeier, Chem. Mater. 10 (1998) 2753–2769.
[21] I.G. Casella, M. Gatta, M. Contursi, J. Electroanal. Chem. 561 (2004) 103–111.
[22] C. Su, A. Lu, Y. Xu, F. Chen, A. Khlobystov, L. Li, ACS Nano 5 (2011) 2332–2359.
[23] S.A. Waghuley, S.M. Yenorkar, S.S. Yawale, S.P. Yawale, Sens. Actuators B Chem. 128 (2008) 366–373.
[24] Y. Wu, B. Wang, Y. Ma, Y. Huang, N. Li, F. Zhang, Y. Chen, Nano. Res. 3 (2010) 661–669.
[25] D.S. Dhawale, R.R. Salunkhe, V.J. Fulari, M.C. Rath, S.N. Sawant, C.D. Lokhande, Sens. Actuators B 141 (2009) 58–64.
[26] D.V. Tuan, A. Kumar, S. Roche, F. Ortmann, M.F. Thorpe, P. Ordejon, Phys. Rev. B 86 (2012) 121,408.
[27] J. Kotakoski, A.V. Krasheninnikov, U. Kaiser, J.C. Meyer, Phys. Rev. Lett. 106 (2011) 105,505.
[28] Z. Ni, Y. Wang, T. Yu, Z. Shen, Nano Res. 1 (2008) 273–291.
[29] C. Thomsen, S. Reich, Phys. Rev. Lett. 85 (2000) 5214.
[30] N.K. Memon, S.D. Tse, J.F. Al-Sharab, H. Yamaguchi, A.B. Goncalves, B.H. Kear, Y. Jaluria, E.Y. Andrei, M. Chhowalla, Carbon 49 (2011) 5064–5070.
[31] A.S. Patole, S.P. Patole, H. Kang, J. Yoo, T. Kim, J. Ahn, J. Colloid Interface Sci. 350 (2010) 530–537.
[32] F. Schroder, N. Bagdassarov, F. Ritter, L. Bayarjargal, Phase Transit. 83 (2010) 311–325.
[33] O. Lupan, V.V. Ursaki, G. Chai, L. Chow, G.A. Emelchenko, I.M. Tiginyanu, A.N. Gruzintsev, A.N. Redkin, Sens. Actuators B 144 (2010) 56–66.
[34] S. Pati, S.B. Majumder, P. Banerji, J. Alloys Compounds 541 (2012) 376–379.
[35] L.K. Bangal, J.Y. Patil, I.S. Mulla, S.S. Suryavanshi, Ceramics Int. 38 (2012) 4835–4844.
[36] R.A. Marcus, Can. J. Chem. 37 (1959) 155–163.
[37] V.D. Kapase, S.A. Ghosh, G.N. Chaudhari, F.C. Raghuwanshi, Talenta 76 (2008) 610–616.
[38] B.C. Yadav, S. Singh, A. Yadav, Appl. Surf. Sci. 257 (2011) 1960–1966.
[39] D. Patil, V. Patil, P. Patil, Sens. Actuators B 152 (2011) 299–306.
[40] R.R. Salunkhe, D.S. Dhawale, U.M. Patil, C.D. Lokhande, Sens. Actuators B 136 (2009) 39–44.